



# Monodisperse nickel-nanoparticles for stereo- and chemoselective hydrogenation of alkynes to alkenes

Kathiravan Murugesan<sup>a</sup>, Ahmad S. Alshammari<sup>b</sup>, Manzar Sohail<sup>a</sup>, Matthias Beller<sup>a,\*</sup>, Rajenahally V. Jagadeesh<sup>a,\*</sup>

<sup>a</sup> Leibniz-Institut für Katalyse e. V. an der Universität Rostock, Albert Einstein-Str. 29a, 18059 Rostock, Germany

<sup>b</sup> King Abdulaziz City for Science and Technology, Riyadh 11442, Saudi Arabia

## ARTICLE INFO

### Article history:

Received 3 September 2018

Revised 30 November 2018

Accepted 17 December 2018

### Keywords:

Ni-nanoparticles

Monosaccharides

Hydrogenation

Alkynes

Alkenes

## ABSTRACT

Here, we report the use of monosaccharides for the preparation of novel nickel nanoparticles (NP), which constitute selective hydrogenation catalysts. For example, immobilization of fructose and Ni(OAc)<sub>2</sub> on silica and subsequent pyrolysis under inert atmosphere produced graphitic shells encapsulated Ni-NP with uniform size and distribution. Interestingly, fructose acts as structure controlling compound to generate specific graphitic layers and the formation of monodisperse NP. The resulting stable and reusable catalysts allow for stereo- and chemoselective semihydrogenation of functionalized and structurally diverse alkynes in high yields and selectivity.

© 2019 The Author(s). Published by Elsevier Inc. This is an open access article under the CC BY license (<http://creativecommons.org/licenses/by/4.0/>).

## 1. Introduction

The valorization of renewable resources for the production of chemicals, materials, energy and life science molecules continues to be an important goal of chemical research [1]. Among the feedstocks, simple monosaccharides such as glucose, fructose, galactose and mannose serve as primary energy source in most of organisms, from bacteria to humans [2]. In the past decade, some of these sugars, especially fructose and glucose, became interesting for the production of platform chemicals such as 5-hydroxymethylfurfural (5-HMF), levulinic acid (LA), formic acid (FA), acetic acid and furfural [1c,3]. Compared to synthetic valorizations, the utilization of monosaccharides for the preparation of nano-scale materials and catalysts is less explored [1–4]. In general, a majority of such materials were prepared by direct pyrolysis of biomass, which acted as self-sacrificing support, along with metal salts [5,6]. However, achieving stable nanoparticles with controlled size and uniform distribution still remains challenging in these processes [4,5]. To overcome these limitations, here we describe the preparation of monodisperse nickel nanoparticles from monosaccharide-Ni acetate templates on silica and subsequent pyrolysis. As a result, graphitic shells encapsulated highly

stable Ni-nanoparticles with identical size (6 nm) and even distribution are produced, which constitute reusable and highly selective hydrogenation catalysts for the conversion of alkynes to alkenes.

The hydrogenation of alkynes to alkenes is a versatile and environmentally benign process applied in both research laboratories and industries [6]. In the latter case, this transformation is used to “purify” bulk alkenes, which serve as central intermediates in the chemical and petrochemical industries [6a,7]. Noteworthy, stereo selective access to either E- or Z-alkenes, which are found to be the integral parts of numerous biologically active compounds, is important in synthetic organic chemistry and drug discovery [6a,8]. Regarding the catalysts for this transformation, the so-called Lindlar catalyst (Pd/CaCO<sub>3</sub> poisoned with Pb(OAc)<sub>2</sub> and quinoline) constitutes an industrially used state-of-the-art-system to produce Z-alkenes [9]. However, other precious metal catalysts based on Ru [10a–10d], Pd [10e–10g] and Au [10h,10i] have been also disclosed for the semihydrogenation of alkynes. In addition to precious metal catalysts, in recent years Fe-[11a–11d], Co-[11e–11g], Ni-[11h–11j], Cu-[11k] and V-[11l] based both homogeneous [11a,11b,11f,11i] and heterogeneous [11c–11e,11g–11j] catalysts have also been developed for this process. Despite all these achievements, the development of practical base-metal catalysts for chemo- and stereo-selective semihydrogenation of structurally challenging alkynes is still desired.

\* Corresponding authors.

E-mail addresses: [matthias.beller@catalysis.de](mailto:matthias.beller@catalysis.de) (M. Beller), [jagadeesh.jajenahally@catalysis.de](mailto:jagadeesh.jajenahally@catalysis.de) (R.V. Jagadeesh).

## 2. Experimental section

### 2.1. Materials and methods

All substrates were obtained commercially from various chemical companies and the purity has been checked before using. Nickel(II) acetate tetrahydrate (cat no. 379883-10G), D-(–)-Fructose (cat no F0127-500G), D-(+)-Glucose (cat no G8270-100G), D-(+)-Mannose (cat no 3458-28-4), D-(+)-Galactose (cat no G0750-10G) were purchased from Sigma-Aldrich Acetonitrile (ACN, code- 149520010; 99%) was obtained from Across Chemicals. Silica (Aerosil OX-50) was obtained from Evonik. The pyrolysis experiments were carried out in Nitech-Qex oven.

The TEM measurements were performed at 200 kV with an aberration-corrected JEM-ARM200F (JEOL, Corrector: CEOS). The microscope is equipped with a JED-2300 (JEOL) energy-dispersive x-ray-spectrometer (EDXS) and an Enfinum ER (GATAN) with Dual EELS for chemical analysis. The aberration corrected STEM imaging (High-Angle Annular Dark Field (HAADF) and Annular Bright Field (ABF)) were performed under the following conditions. HAADF and ABF both were done with a spot size of approximately 0.1 nm, a convergence angle of 30–36° and collection semi-angles for HAADF and ABF of 90–170 mrad and 11–22 mrad respectively. Dual EELS was done at a CL of 4 cm, an illumination semi angle of 21.3 mrad and an entrance aperture semi angle of 19.8 mrad. The solid samples were deposited without any pretreatment on a holey carbon supported Cu-grid (mesh 300) and transferred to the microscope. The average particle diameter and size distribution were calculated using Java image tool software (ImageJ), based on the data of an average of 100–200 particles. XRD powder patterns were recorded on a Stoe STADI P diffractometer, equipped with a linear Position Sensitive Detector (PSD) using Cu K $\alpha$  radiation ( $\lambda = 1.5406 \text{ \AA}$ ). Processing and assignment of the powder patterns was done using the software WinXpow (Stoe) and the Powder Diffraction File (PDF) database of the International Centre of Diffraction Data (ICDD). X-ray photoelectron spectroscopy (XPS) analysis were carried out in a PHI 5000 VersaProbe Scanning ESCA microprobe (ULVAC-PHI, Japan/USA) instrument at a base pressure of  $5.5 \times 10^{-7} \text{ Pa}$ . X-ray source of Al-K $\alpha$  ( $h\nu = 1486.6 \text{ eV}$ ) with spot size of  $200 \text{ }\mu\text{m}$  has been used. The analyzer of 187.850 eV was used with the power of 25 W at pass energy 180 eV with a 0.4 eV energy step, and the core-level spectra were acquired 10 at pass energy 58.70.5 eV with a 0.5 eV energy step. For quantitative analysis the peaks were deconvoluted with Gaussian-Lorentzian curves using CasaXPS software, the peak area was divided by a sensitivity factor obtained from the element specific Scofield factor and the transmission function of the spectrometer. N<sub>2</sub> physisorption analysis at  $-196 \text{ }^\circ\text{C}$  was recorded using a Micromeritics ASAP 2020 analyzer. Prior to analysis, approximately 0.1–0.15 g of each catalyst sample was outgassed for 4 h at  $250 \text{ }^\circ\text{C}$  in an atmosphere of N<sub>2</sub>. The total specific surface area, pore volume, and pore size were analyzed by single or multi-point BET methods. CO chemisorption experiments were performed by using a Micromeritics AutoChem II 2920. Experiments were conducted at  $30 \text{ }^\circ\text{C}$  by injecting 10% CO/Ar into the reduced catalyst bed. Pulses were injected by means of a calibrated sample loop (Vloop = 1 mL).

All catalytic experiments were carried out in 300 mL and 100 mL autoclaves (PARR Instrument Company). In order to avoid unspecific reactions, all catalytic reactions were carried out either in glass vials, which were placed inside the autoclave, or glass/Teflon vessel fitted autoclaves. GC and GC-MS were recorded on Agilent 6890N instrument.

GC conversion and yields were determined by GC-FID, HP6890 with FID detector, column HP530  $m \times 250 \text{ mm} \times 0.25 \text{ }\mu\text{m}$ . 1H, 13C

NMR data were recorded on a Bruker ARX 300 and Bruker ARX 400 spectrometers using DMSO  $d_6$ , CD<sub>3</sub>OD and CDCl<sub>3</sub> solvents.

### 2.2. Preparation of Ni-fructose@SiO<sub>2</sub> template and pyrolysis to obtain nanomaterial

In a 50 mL round bottomed flask, D-fructose (800.2 mg) in 20 mL distilled water (H<sub>2</sub>O) was stirred for 2–3 min at  $100 \text{ }^\circ\text{C}$  and then nickel (II) acetate tetrahydrate (381.57 mg) was added. Then, the round bottomed flask containing reaction mixture was placed into an aluminum block preheated at  $100 \text{ }^\circ\text{C}$  and stirred for 20–30 min by fixing reflux condenser. Then, 1.2 g of silica (Aerosil-OX-50) was added followed by the addition of 15 mL H<sub>2</sub>O and the reaction mixture again was stirred at  $100 \text{ }^\circ\text{C}$  for 4–5 h by fixing reflux condenser. Then, the reflux condenser was removed and the round bottomed flask containing reaction products were allowed to stand without stirring and closing for 20 h at  $100 \text{ }^\circ\text{C}$  in order to slow evaporation of H<sub>2</sub>O. After the evaporation of solvent and ensuring the complete drying, the material was cooled to room temperature and grinded to fine powder. The powdered material was pyrolyzed at the defined temperature ( $600 \text{ }^\circ\text{C}$ ,  $800 \text{ }^\circ\text{C}$  and  $1000 \text{ }^\circ\text{C}$ ) for 2 h under an argon atmosphere and then cooled to room temperature after pyrolysis. Ni-materials (Ni-monosaccharide-SiO<sub>2</sub>-800) using other monosaccharides such as glucose, mannose and galactose were also prepared using the same procedure.

Elemental analysis of Ni-fructose@SiO<sub>2</sub>-800: Ni = 4.8 wt%, Si = 34.41 wt%, C = 7.34 wt% and H = 0.05 wt%.

## 3. Results and discussion

We started our investigations by the preparation of novel Ni-nanoparticles (Ni-NP) using simple fructose and Ni-acetate as precursors. First, we created a Ni-fructose template on SiO<sub>2</sub> by mixing the components in water and refluxing them at  $100 \text{ }^\circ\text{C}$ . After slow evaporation of water and drying, the template was formed (Fig. 1). Subsequently, this templated solid compound was pyrolyzed at  $800 \text{ }^\circ\text{C}$  under argon atmosphere (Fig. 1). In addition to fructose, Ni-NP was also prepared using other monosaccharides such as glucose, galactose and mannose under similar conditions. Hereafter, these Ni-materials are labelled as Ni-monosaccharide@SiO<sub>2</sub>-x, where x defines the pyrolysis temperature.

All the prepared new materials were tested for the hydrogenation of diphenylacetylene as benchmark reaction (Table 1). We were surprised to find that all of the catalysts prepared using different monosaccharides showed excellent activity and selectivity to produce > 94% of stilbene with selectivities of 99% for the Z-isomer (Table 1; entries 1–4). Variation of the pyrolysis temperature between 600 and  $1000 \text{ }^\circ\text{C}$ , revealed good activity for the material pyrolyzed at  $600 \text{ }^\circ\text{C}$ , while higher temperature resulted in a less active catalyst (Table 1; entries 5–6). Pyrolysis of simple nickel acetate on silica (Ni@SiO<sub>2</sub>-800) resulted in a significantly less

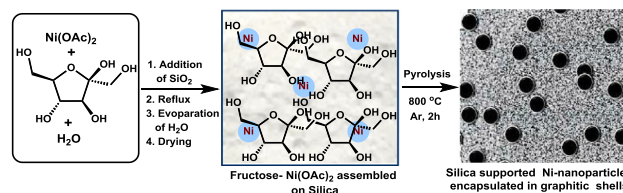
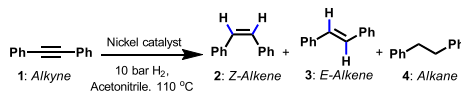


**Fig. 1.** Preparation of graphitic shells encapsulated Ni-nanoparticles supported on silica by the pyrolysis of nickel acetate-fructose-SiO<sub>2</sub> template.

**Table 1**  
Hydrogenation of diphenylacetylene: Activity and selectivity of Ni-catalysts.<sup>a</sup>



Entry	Catalyst	Conv (%)	Yield of alkene (%)	Selectivity (Z:E)	Yield of alkane (%)
1	Ni-fructose@SiO <sub>2</sub> -800	>99	94	99:1	5
2	Ni-glucose@SiO <sub>2</sub> -800	>99	94	99:1	5
3	Ni-mannose@SiO <sub>2</sub> -800	>99	94	99:1	5
4	Ni-galactose@SiO <sub>2</sub> -800	>99	94	99:1	5
5	Ni-fructose@SiO <sub>2</sub> -600	88	82	97:3	6
6	Ni-fructose@SiO <sub>2</sub> -1000	60	51	97:3	5
7	Ni@SiO <sub>2</sub> -800	27	25	99:1	–
8	Ni + fructose@SiO <sub>2</sub>	<2	<1	–	–
9	Ni(OAc) <sub>2</sub> + Fructose	<2	<1	–	–

Reaction conditions: 0.5 mmol of diphenylacetylene, 10 mg of catalyst (1.6 mol% Ni), 10 bar H<sub>2</sub>, 2 mL acetonitrile, 110 °C, 15 h, yields were determined by GC using n-hexadecane standard.

active catalyst (Table 1; entry 7). Notably, all the non-pyrolyzed catalysts are completely inactive (Table 1, entries 8–9).

In order to know the structural features as well as to understand the activity and selectivity of these novel materials, detailed characterization by HRTEM (high resolution transmission electron microscopy), EDX (energy-dispersive X-ray spectroscopy), XRD (X-ray powder diffraction) and XPS (X-ray photoelectron spectroscopy) were performed. TEM analysis of the most active catalyst (Ni-fructose@SiO<sub>2</sub>-800) revealed the formation of identical monodisperse metallic Ni-nanoparticles with size of 6 nm (Fig. 2a and Fig. 3). Interestingly all of these particles are surrounded by 3–4 thin layers of graphitic shells (Fig. 2b). The HRTEM image (Fig. 2c) displays the polycrystalline structure and its selected lattice fringe has a distance of 0.18 nm. Fig. 2d shows the selected area of electron diffraction (SAED) patterns. The observed concentric rings indicate the formation of well-crystallized Ni-particles. The deep rings noticed in the pattern corresponds to the reflection of the (1 1 1), (2 0 0), and (2 2 0) planes, which is in line with the results obtained using XRD. Increasing the pyrolysis temperature to 1000 °C, the catalyst becomes less active (Ni-fructose@SiO<sub>2</sub>-1000). This material contains completely metallic Ni, but in less quantity compared to Ni-fructose@SiO<sub>2</sub>-800 (Fig. 4). In addition, the nanoparticles are surrounded by thicker (6–10 layers) graphitic shells (Fig. 4b). The less active material (Ni(OAc)<sub>2</sub>@SiO<sub>2</sub>-800) prepared without D-fructose contains a mixture of nickel oxide- (NiO) and metallic Ni-nanoparticles with wider size distribution ranging between 5 and 35 nm (Fig. 5).

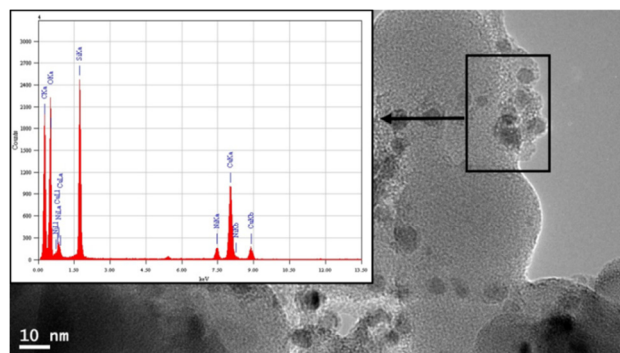


Fig. 3. EDX spectrum of Ni-fructose@SiO<sub>2</sub>-800.

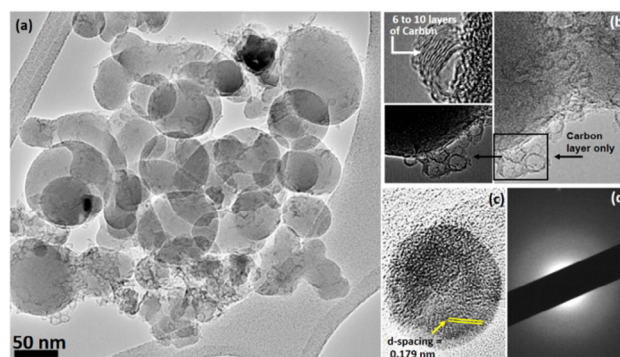
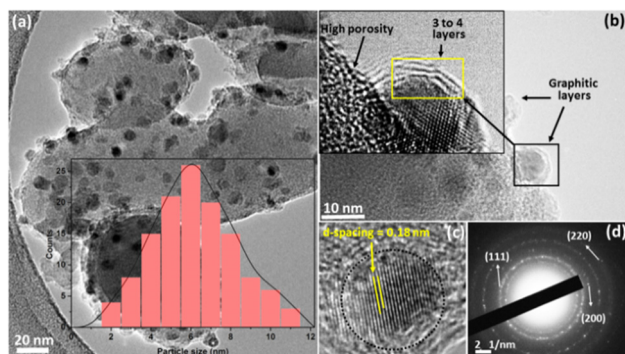


Fig. 4. TEM images of Ni-fructose@SiO<sub>2</sub>-1000 material.



**Fig. 2.** TEM images of Ni-fructose@SiO<sub>2</sub>-800 catalyst. (a) = Monodisperse Ni-NP, (b) = Ni-NP encapsulated within graphitic shells. (c) = Crystal planes of Ni-NP and (d) = selected area electron diffraction (SAED) of Ni-NP.

As observed in Fig. 5a, several nano-sized particles appeared to be attached and agglomerate to form a flower-like shape. All of these nanoparticles are not surrounded by graphitic shells. The different phases of Ni in both active and less active catalysts are also confirmed by the XRD data (Fig. S1), which is in agreement to the TEM analysis. Further, XPS analysis was carried out to elucidate the chemical states of the elements. The survey scan of most active catalyst (Ni-fructose@SiO<sub>2</sub>-800) showed the presence of Ni, C, O and Si elements (Figs S3–S6). After deconvolution, the peaks present at BE 852.9 eV (Ni2p3/2) and BE 870.5 eV (Ni2p1/2) indicate the presence of metallic Ni near the surface (Fig. S2). In addition, the presence of a small quantity of Ni(II) is also evident by the peaks at BE



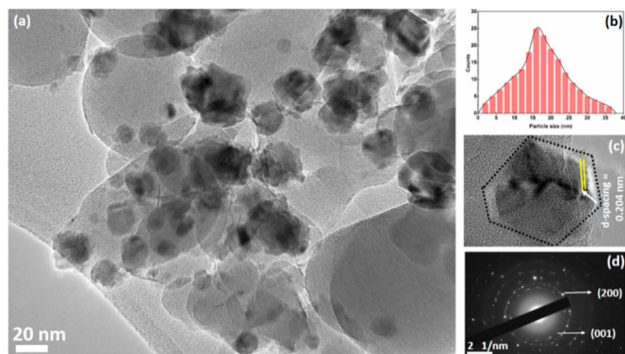
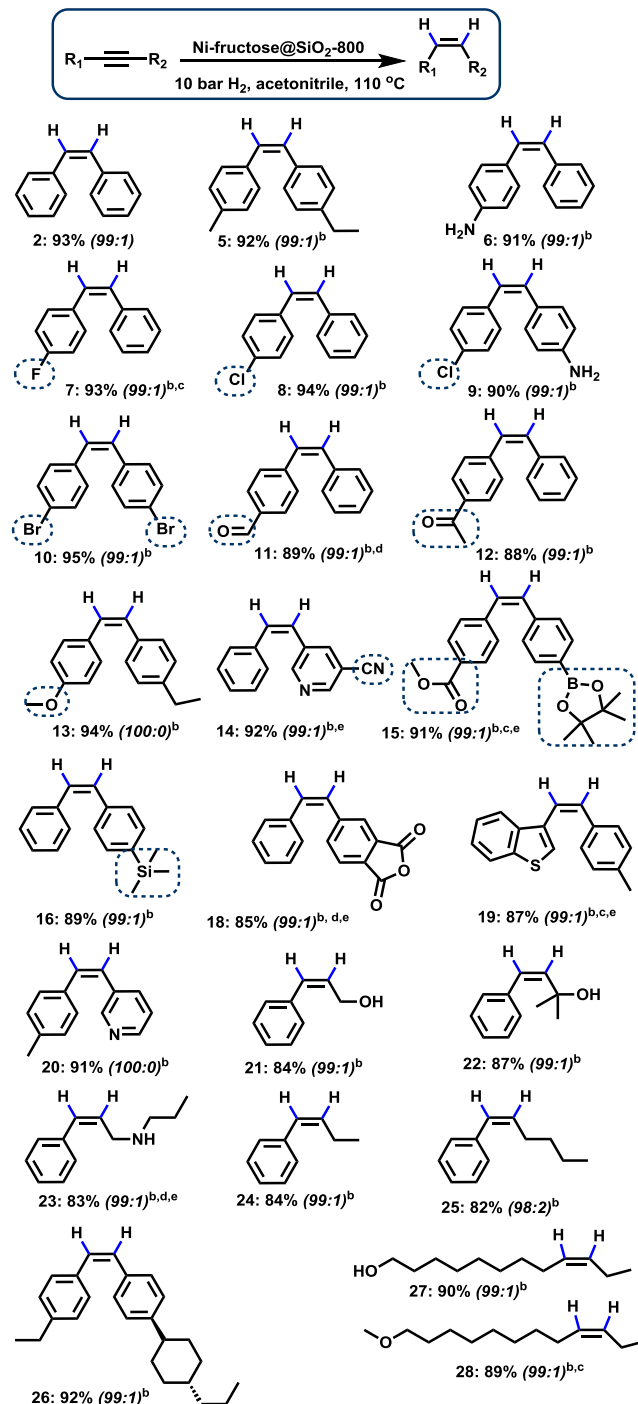


Fig. 5. TEM images of Ni(OAc)<sub>2</sub>@SiO<sub>2</sub> material.

855.1 eV (Ni2p<sub>3/2</sub>) and BE 874.9 eV (Ni2p<sub>1/2</sub>). The peak assigned at BE 858.7 eV, which is of 5.8 eV higher than the Ni2p<sub>3/2</sub> main peak is due to surface and bulk plasmon loss of Ni(0) [12a]. The high resolution XPS spectrum of C1s electrons were deconvoluted into three peaks centered at BE 284.8, 286.1 and a broad peak at 286.9 eV. These three, peaks can be assigned to graphitic carbon C=C/C—C, C—O and C interacting with Ni atoms, respectively (S4) [12a,12b]. The O1s spectrum shows the presence of one type of O predominantly, which obviously stems from SiO<sub>2</sub> and is centered at 532.1 eV BE (Fig. S4) [12c]. Another small peak centered at 534 eV could be assigned to C—O [12b]. The Si2p spectrum shows the presence of only one type of Si (Fig. S5). The asymmetric shape of the Si2p peak is due to overlapping of Si2p<sub>3/2</sub> and Si2p<sub>1/2</sub> [12c]. In the less active (Ni-fructose@SiO<sub>2</sub>-1000) catalyst, only trace of Ni is present at the surface (Fig. S2). Further to know the surface properties of the catalysts, we conducted BET and chemisorption studies. As shown in Table S1, the BET surface area of the catalyst increased from 149.3 to 239.7 m<sup>2</sup>/g with increasing the pyrolysis temperature from 800 to 1000 °C. The CO chemisorption studies indicate that the metal dispersion is increased in case of Ni-fructose@SiO<sub>2</sub>-800 (49.5%) compared to that of Ni-fructose@SiO<sub>2</sub>-1000 (6.2%). All these characterization results evidence that the most active catalyst (Ni-fructose@SiO<sub>2</sub>-800) is characterized by the formation of defined metallic Ni-nanoparticles, which are encapsulated within graphitic shells. Interestingly, fructose generates graphitic layers and allows for the formation of monodisperse Ni-nanoparticles.

After having successfully developed an active catalyst (Ni-fructose@SiO<sub>2</sub>-800), we were interested in its general applicability for the semi-hydrogenation of both internal and terminal alkynes. As shown in Scheme 1, aromatic, heterocyclic and aliphatic internal alkynes were selectively semi-hydrogenated to produce alkenes in good to excellent yields. In all these cases high stereo-selectivity with 98–100% for the Z-isomer formation was achieved (Scheme 1).

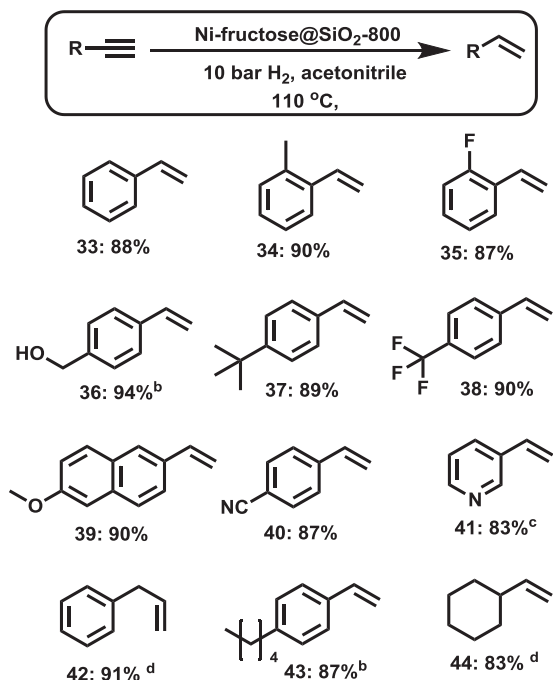
In addition, the novel catalyst showed a high degree of chemoselectivity. Different sensitive halogenated and functionalized alkynes were reduced to the corresponding olefins in up to 95% without any significant dehalogenations (products 7–10). Remarkably, the alkyne group was selectively semi-hydrogenated also in presence of other reducible groups such as aldehyde, keto, nitrile and ester (Scheme 1; products 11–12, 14–15). Thus, our Ni catalyst exhibits both excellent regio- and chemoselectivity. In addition, propargylic alkynes were reduced to produce allylic compounds in up to 87% yields. Apart from aromatic substrates, aliphatic alkynes have also been transformed to the corresponding alkenes in high yields and



**Scheme 1.** Ni-fructose@SiO<sub>2</sub>-800 catalyzed hydrogenation of internal alkynes to Z-alkenes<sup>a</sup>. <sup>a</sup>Reaction conditions: 1 mmol substrate, 30 mg catalyst (2.5 mol% Ni), 10 bar H<sub>2</sub>, 2 mL acetonitrile, 110 °C, 15 h, isolated yields. <sup>b</sup>Z: E isomeric ratios were determined by NMR and GC-MS. <sup>c</sup>24 h. <sup>d</sup>2 mL dioxane solvent, <sup>e</sup>60 mg catalyst (5 mol% Ni).

selectivities (Scheme 1; products 27–28). Next, the hydrogenation of terminal alkynes was performed. Similar to internal alkynes, here the C—C triple bond was selectively transformed to C—C double bond in both aromatic and aliphatic compound (Scheme 2).

Furthermore, to showcase the generality and selectivity of our novel Ni-based nano-catalyst, its reactivity was compared with the Lindlar catalyst. For this purpose, the hydrogenation of 3

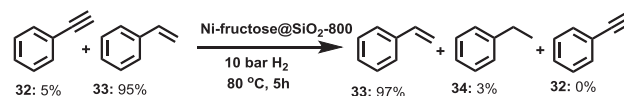


**Scheme 2.** Semi-hydrogenation of terminal alkynes using Ni-fructose@SiO<sub>2</sub>-800 catalyst<sup>a</sup>. <sup>a</sup>Reaction conditions: 1 mmol substrate, 8 mg catalyst (0.6 mol% Ni), 10 bar H<sub>2</sub>, 2 mL acetonitrile, 110 °C, 5 h. Yields were determined by GC using n-hexadecane as standard. <sup>b</sup>Isolated yields. <sup>c</sup>15 h. <sup>d</sup>15 mg catalyst (1.2 mol% Ni).

selected functionalized alkynes (29–31) was carried out under standard reaction conditions. As shown in Table 2, the Lindlar catalyst showed no activity for the hydrogenation of 5-(phenylethynyl)nicotinonitrile (29) and the ester-substituted diphenylacetylene (30). Although it exhibited excellent activity for the hydrogenation of bis(4-bromophenyl)acetylene (31), significant debromination occurred. Noteworthy, Ni-fructose@SiO<sub>2</sub>-800 successfully worked for the semi-hydrogenation of all these substrates.

After having established the synthetic utility, selectivity and generality of this novel Ni-catalyst, the practical applicability was demonstrated by the hydrogenation of a small quantity of alkyne in presence of excess of alkene.

As pointed out in the introduction, the removal of alkyne impurities from alkenes is highly essential for the valorization of bulk olefins. Using Ni-fructose@SiO<sub>2</sub>-800, 0.5 mmol of phenylacetylene (32) was hydrogenated in presence of 9.5 mmol styrene (33) at 80 °C with 10 bar H<sub>2</sub> (Scheme 3). Under these reaction conditions, phenylacetylene was completely converted to produce 97% of styrene and only 3% of ethylbenzene were obtained.



**Scheme 3.** Selective hydrogenation of phenylacetylene in the presence of styrene using Ni-fructose@SiO<sub>2</sub>-800 showcasing the purification of alkenes. Reaction conditions: 0.5 mmol phenylacetylene, 9.5 mmol styrene, 80 mg catalyst (0.6 mol % Ni), 10 bar H<sub>2</sub>, 15 mL acetonitrile, 80 °C, 5 h.

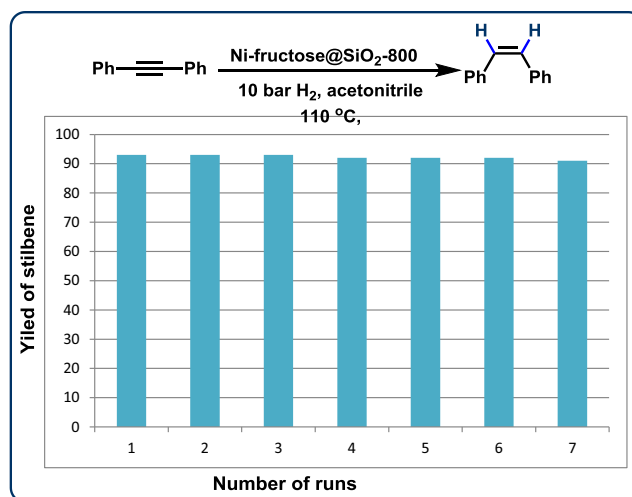


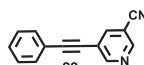
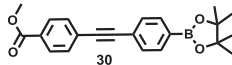
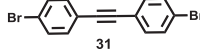
**Fig. 6.** Recycling of Ni-fructose@SiO<sub>2</sub>-800 for the hydrogenation of diphenylacetylene to Z-stilbene. Reaction conditions: 10 mmol diphenylacetylene 100 mg catalyst (1.5 mol% Ni), 10 bar H<sub>2</sub>, 15 mL acetonitrile, 110 °C, 15 h, GC-yields, in all the cases selectivity = 99:1 (Z: E).

Finally, the recycling and reusability of the optimal catalyst was investigated. Indeed, Ni-fructose@SiO<sub>2</sub>-800 was highly stable under the applied conditions and was successfully recycled and reused up to 6 times without any significant loss of both activity and selectivity (Fig. 6).

#### 4. Conclusion

In conclusion, we demonstrate the use of inexpensive monosaccharides for the controlled preparation of base metal nanoparticles as sustainable selective hydrogenation catalysts. The immobilization and pyrolysis of fructose and nickel acetate on silica produces stable and reusable monodisperse Ni-nanoparticles encapsulated in graphitic shells. These nanoparticles enable the hydrogenation of a series of functionalized and structurally diverse aromatic, heterocyclic and aliphatic alkynes to the corresponding alkenes with excellent stereo- (98–100% Z-alkene formation) and chemo-selectivity.

**Table 2**  
Hydrogenation of selected substrates with Ni-fructose@SiO<sub>2</sub>-800 and Lindlar catalyst: Comparison of reactivity and selectivity.

Alkyne	Catalyst	Conv. (%)	Yield of alkene (%)	Selectivity (Z:E)
 <p>29</p>	Ni-fructose @SiO <sub>2</sub> -800	>99%	92%	99:01
	Lindlar catalyst	<1	<1	–
 <p>30</p>	Ni-fructose @SiO <sub>2</sub> -800	>99%	91%	99:01
	Lindlar catalyst	<2	<1	–
 <p>31</p>	Ni-fructose @SiO <sub>2</sub> -800	>99%	95%	99:01
	Lindlar catalyst	>99	65%	99:01
		30% mono debrominated alkene		

Reaction conditions: 1 mmol substrate, 2.5 mol% catalyst, 10 bar H<sub>2</sub>, 2 mL acetonitrile, 110 °C, 15 h.

## Note

The authors declare no conflict of interest.

## Acknowledgements

We gratefully acknowledge the European Research Council (EU project 670986-NoNaCat), King Abdulaziz City for Science and Technology and the State of Mecklenburg-Vorpommern for financial and general support. We thank the analytical team of the Leibniz-Institute for Catalysis, Rostock for measuring NMR data.

## Appendix A. Supplementary material

Supplementary data to this article can be found online at <https://doi.org/10.1016/j.jcat.2018.12.018>.

## References

- [1] a) C.O. Tuck, E. Pérez, I.T. Horváth, R.A. Sheldon, M. Poliakoff, *Science* 337 (2012) 695–699;  
b) D. Klass, *Biomass for Renewable Energy, Fuels, and Chemicals*, Academic Press, 1998;  
c) A. Corma, S. Iborra, A. Velty, *Chem. Rev.* 107 (2007) 2411–2502;  
d) Z. Sun, B. Fridrich, A. de Santi, S. Elangovan, K. Barta, *Chem. Rev.* 118 (2018) 614–678;  
e) P.C.A. Bruijninx, B.M. Weckhuysen, *Nat. Chem.* 6 (2014) 1035–1036;  
f) R. Rinaldi, *Catalytic Hydrogenation for Biomass Valorization*, Royal Society of Chemistry, 2015.
- [2] a) Z. Gyorgydeak, I. Pelyvas, *Monosaccharide Sugars*, Academic Press, 1997;  
b) P.C. Collins, R.J. Ferrier, *Monosaccharides: Their Chemistry and Their Roles in Natural Products*, Wiley, 1995;  
c) R. Stick, S. Williams, *Carbohydrates: The Essential Molecules of Life*, Elsevier, 2008.
- [3] a) R.S. Assary, T. Kim, J.J. Low, J. Greeley, L.A. Curtiss, *Phys. Chem. Chem. Phys.* 14 (2012) 16603–16611;  
b) Y.R. Leshkov, C.J. Barrett, Z.Y. Liu, J.A. Dumesic, *Nature* 447 (2007) 982–985;  
c) Zhen Fang, R.L. Smith, X. Qi Jr., *Production of Platform Chemicals from Sustainable Resources*, Springer, 2017.
- [4] a) M. Marradi, I. García, S. Penadés, *Prog. Mol. Biol. Transl. Sci.* 104 (2011) 141–173;  
b) Z.-H. Miao, H. Wang, H. Yang, Z. Li, L. Zhen, C.-Y. Xu, *ACS Appl. Mater. Interf.* 8 (2016) 15904–15910;  
c) M. Mahyari, A. Shaabani, M. Behbahani, A. Bagheri, *App. Organomet. Chem.* 28 (2014) 576–583;  
d) J.C. Heckel, F.F. Farhan, G. Chumanov, *Coll. Poly. Sci.* 286 (2008) 1545–1552;  
e) M. Taleb, J. Nerut, T. Tooming, T. Thomberg, E. Lust, *J. Electrochem. Soc.* 163 (2016) 1251–1257;  
f) S. Kasakov, C. Zhao, E. Barath, Z.A. Chase, J.L. Fulton, D.M. Camaioni, A. Vjunov, H. Shi, J.A. Lercher, *Chem. Europ. J.* 21 (2015) 1567–1577;  
g) D. Zhu, H. Jiang, L. Zhang, H. Zheng, Xueli, H. Fu, M. Yuan, H. Chen, R. Li, *ChemCatChem* 6 (2014) 2954–2960;  
h) J.E. Camp, J.J. Dunsford, E.P. Cannons, W.J. Restorick, A. Gadzhieva, M.W. Fay, R.J. Smith, *ACS Sustain. Chem. Eng.* 2 (2014) 500–505.
- [5] a) E. Guibal, *Prog. Polym. Sci.* 30 (2005) 71–109;  
b) B. Sahoo, A.-E. Surkus, M.-M. Pohl, J. Radnik, M. Schneider, S. Bachmann, M. Scalone, K. Junge, M. Beller, *Angew. Chem. Int. Ed.* 56 (2017) 11242–11247.
- [6] a) C. Oger, L. Balas, T. Durand, J.-M. Galano, *Chem. Rev.* 113 (2013) 1313–1350;  
b) J.A. Delgado, O. Benkirane, C. Claver, D. Curulla-Ferré, C. Godard, *Dalton Trans.* 46 (2017) 12381–12403;  
c) H.-U. Blaser, A. Schnyder, H. Steiner, F. Rössler, P. Baumeister, *Handbook of Heterogeneous Catalysis*, Wiley–VCH, 2008;  
d) C.J. J.G. de Vries, *Elsevier Handbook of Homogeneous Hydrogenation*, Wiley–VCH, 2007.
- [7] a) S. Patai, *The Chemistry of Alkenes*, Interscience, 1964;  
b) T.E. Müller, K.C. Hultsch, M. Yus, F. Foubelo, M. Tada, *Chem. Rev.* 108 (2008) 3795–3892;  
c) R. Remy, C.G. Bochet, *Chem. Rev.* 116 (2016) 9816–9849;  
d) X.-F. Wu, X. Fang, L. Wu, R. Jackstell, H. Neumann, M. Beller, *ACC Chem. Res.* 47 (2014) 1041–1053;  
e) R.H. Grubbs, A.G. Wenzel, D.J. O’Leary, E. Khosravi, *Handbook of Metathesis*, Wiley–CH, Weinheim, Germany, 2015.
- [8] a) J. Wang, *Stereoselective Alkene Synthesis*, Springer, 2012;  
b) W.-Y. Siau, Y. Zhang, Y. Zhao, *Top. Curr. Chem.* 327 (2012) 33–58;  
c) S. Fu, N. Chen, X. Liu, Z. Shao, S.-P. Luo, Q. Liu, *J. Am. Chem. Soc.* 138 (2016) 8588–8594;  
d) B.E. Maryanoff, A.B. Reitz, *Chem. Rev.* 89 (1989) 863;  
e) W. Wadsworth, W.D.J. Emmons, *J. Am. Chem. Soc.* 8 (1961) 1733.
- [9] a) H. Lindlar, *Helv. Chim. Acta* 35 (1952) 446–450;  
b) H. Lindlar, R. Dubuis, *Org. Synth.* 46 (1966) 89–91.
- [10] a) K. Radkowski, B. Sundararaju, A. Fürstner, *Angew. Chem. Int. Ed.* 52 (2013) 355–360;  
b) A. Guthertz, M. Leutzsch, L.M. Wolf, P. Gupta, S.M. Rummelt, R. Goddard, C. Farès, W.R. Thiel, A. Fürstner, *J. Am. Chem. Soc.* 140 (2018) 3156–3169;  
c) K.T. Neumann, S. Klimczyk, M.N. Burhardt, B.B.-. Andersen, T. Skrydstrup, A. T. Lindhard, *ACS Catal.* 6 (2016) 4710–4714;  
d) R. Kusy, K. Grela, *Org. Lett.* 18 (2016) 6196–6199;  
e) O. Verho, H. Zheng, K.P.J. Gustafson, A. Nagendiran, X. Zou, J.-E. Bäckvall, *ChemCatChem* 8 (2016) 773–778;  
f) Y. Lu, X. Feng, B.S. Takale, Y. Yamamoto, W. Zhang, M. Bao, *ACS Catal.* 7 (2017) 8296–8303;  
g) S. Furukawa, T. Komatsu, *ACS Catal.* 6 (2016) 2121–2125;  
h) J.L. Florio, R.V. Gonçalves, E. Teixeira-Neto, M.A. Ortuño, N. López, L.M. Rossi, *ACS Catal.* 8 (2018) 3516–3524;  
i) Y.S. Wagh, S. Yogesh, N. Asao, *J. Org. Chem.* 80 (2015) 847–851.
- [11] a) D. Srimani, Y. Diskin-Posner, Y. Ben-David, D. Milstein, *Angew. Chem. Int. Ed.* 52 (2013) 14131–14134;  
b) L. Ilies, T. Yoshida, E. Nakamura, *J. Am. Chem. Soc.* 134 (2012) 16951–16954;  
c) T.N. Gieshoff, A. Welther, M.T. Kessler, M.H.G. Precht, A.J.V. Wangelin, *Chem. Commun.* 50 (2014) 2261–2264;  
d) A. Welther, M. Bauer, M. Mayer, A.J.V. Wangelin, *ChemCatChem* 4 (2012) 1088–1093;  
e) F. Chen, C. Kreyenschulte, J. Radnik, H. Lund, A.-E. Surkus, K. Junge, M. Beller, *ACS Catal.* 7 (2017) 1526–1532;  
f) C. Chen, Y. Huang, Z. Zhang, X.-Q. Dong, X. Zhang, *Chem. Commun.* 53 (2017) 4612–4615;  
g) K. Tokmic, A.R. Fout, *J. Am. Chem. Soc.* 138 (2016) 13700–13705;  
h) H. Konnerth, M.H.G. Precht, *Chem. Commun.* 52 (2016) 9129–9132;  
i) M.D. de los Bernardos, S. Pérez-Rodríguez, A. Gual, C. Claver, C. Godard, *Chem. Commun.* 53 (2017) 7894–7897;  
j) F. Alonso, I. Osante, M. Yus, *Adv. Synth. Catal.* 348 (2006) 305–308;  
k) N. Kaeffer, H.-. Ju Liu, H.-K. Lo, A. Fedorov, C. Coperet, *Chem. Sci.* (2018), <https://doi.org/10.1039/c8sc01924j>;  
l) H.S.L. Pierre, J. Arnold, F.D. Toste, *Angew. Chem. Int. Ed.* 50 (2011) 3900–3903.
- [12] a) Y. Feng, X.-Y. Yu, U. Paik, *Sci. Report.* 6 (2016) 34004;  
b) D.H. Wang, Y. Hu, J.J. Zhao, L.L. Zeng, X.M. Taob, W. Chen, *J. Mater. Chem. A* 2 (2014) 17415–17420;  
c) G.M. Bancroft, H.W. Nesbitt, R. Ho, D.M. Shaw, J.S. Tse, M.C. Biesinger, *Phys. Rev. B* 80 (2009) 075405.